Materials Advances

ROYAL SOCIETY OF CHEMISTRY

PAPER

View Article Online
View Journal | View Issue

Cite this: *Mater. Adv.*, 2025, 6, 5914

Prediction of photocatalytic performance of TiO_2 hybrid catalysts based on the nature of the ligand: a simple theoretical model as a guide for advanced materials†

Giuseppe Santoriello, ‡[a] Claudio Imparato, ‡*[b] Ida Ritacco, [a] Aurelio Bifulco, [b] Paola Amato,[b] Gerardino D'Errico, [c] Antonio Aronne, [b] Matteo Farnesi Camellone, [d] Fabia Grisi [a] and Lucia Caporaso*[a]

Received 17th January 2025,
Accepted 1st July 2025

DOI: 10.1039/d5ma00049a

rsc.li/materials-advances

The chemical modification of metal oxide surfaces with organic molecules is a versatile strategy to tune their physicochemical and electronic properties, enhancing their efficiency in a range of applications, including catalysis and light harvesting. Through an integrated theoretical and experimental approach, involving DFT calculations and characterization by spectroscopic techniques, the interaction of different chemical classes of ligands with O-defective TiO_2 surfaces is investigated. A fast method based on QM calculations to predict the steric and electronic stability of the formed Ti–ligand complexes is introduced. It allows assessing the role of organic ligands as structure-directing agents in the synthesis process of these materials and foreseeing their efficiency in the production of photoactive species. The chemical nature of the ligand and its fine structure are key features, driving the synthetic process and leading to different materials in terms of morphology, defectivity, optoelectronic properties and catalytic activity in the generation of reactive oxygen species. The theoretical findings are supported by the characterization of a set of TiO_2-based amorphous gel samples containing different carboxylate ligands, which highlight the effects of the interfacial charge transfer complexes on the ability to produce and stabilize superoxide radicals on the hybrid surfaces.

1. Introduction

The response of semiconducting materials to light has been extensively studied in various fields, such as solar cells,[1–5] water splitting,[6,7] selective organic transformations,[8] CO_2 reduction for fuel generation,[9,10] sensors[11] and pollutant degradation.[12] Among metal oxide semiconductors, titanium dioxide (TiO_2) is considered particularly suitable as a photocatalyst because of its versatility, low cost, abundance, chemical stability, non-toxicity and sustainable features.[13] The photocatalytic reactions on TiO_2 are triggered by band-gap excitation and subsequent generation of electron–hole (e^-/h^+) pairs[14] that can initiate redox reactions on the surface. However, due to its large band gap (~3.2 eV),[15] TiO_2 is activated mainly by UV light, while it is practically inactive under visible light irradiation. Consequently, the utilization of solar radiation as a sustainable energy source is hampered, because only 5% of the incoming solar energy on the Earth's surface is in the UV range.[16] Moreover, the fast recombination of charge carriers reduces the quantum efficiency of photocatalyzed reactions. For these reasons, the photochemical mechanisms and basic principles of photocatalysis on TiO_2 have been extensively studied with the aim of providing important improvements to make photocatalysis a sustainable and feasible process under real environmental conditions.

One of the strategies to design highly active TiO_2 nanomaterials is the chemical modification of the surface[17] to improve charge carrier separation, enable visible light absorption, and enhance photocatalytic activity. These aims can be achieved by doping with heteroatoms, introducing point defects or loading photosensitising ligands onto TiO_2. Defect engineering is increasingly studied since the controlled formation of oxygen vacancies has a significant impact on the optical properties and surface

[a] *Dipartimento di Chimica e Biologia, Università degli Studi di Salerno, via Giovanni Paolo II 132, 84084 Fisciano, Salerno, Italy. E-mail: lcaporaso@unisa.it*
[b] *Dipartimento di Ingegneria Chimica, dei Materiali e della Produzione Industriale, Università degli Studi di Napoli Federico II, Piazzale Tecchio 80, 80125 Naples, Italy. E-mail: claudio.imparato@unina.it*
[c] *Dipartimento di Scienze Chimiche, Università degli Studi di Napoli Federico II, Via Cinthia, 80125 Naples, Italy*
[d] *CNR-IOM, Consiglio Nazionale delle Ricerche – Istituto Officina dei Materiali, c/o SISSA, 34136 Trieste, Italy*

† Electronic supplementary information (ESI) available. See DOI: https://doi.org/10.1039/d5ma00049a

‡ G. S. and C. I. contributed equally to this paper.

reactivity of the resulting sub-stoichiometric titanium oxide.[18] The linkage of ligands on the surface is another interesting approach, as the catalytic and photocatalytic performance of a semiconductor depends on the electronic structure of the surface reaction sites, which can be enhanced by anchoring an organic molecule or a metal complex able to act as a co-catalyst and/or photosensitiser. Among the organic ligands, several classes of small molecules, such as carboxylic acids, diols and diketones, have attracted attention in recent years because of their ability to establish complexes with semiconductors, particularly TiO_2. Such interactions usually involve interfacial charge transfer (CT) between the compound and the semiconductor, the characteristics of which (direction of electron transfer, direct or indirect mechanism, extent of charge separation and delocalisation, *etc.*) are strongly related to the respective frontier energy levels, *i.e.* the potential of the valence and conduction bands of the semiconductor and the HOMO and LUMO of the ligand compound.[19,20] A detailed understanding of the interaction of organic molecules with the TiO_2 surface is crucial for various purposes, as the different strengths and charge-transfer characters of the complexes modify the polar character, wettability, electric charge, light absorption and luminescence, influencing not only the catalytic efficiency but also the adsorption capacity, sensing properties and photoresponsivity of the material.[21–23] Other examples of hybrid materials, whose functionality is determined by the coordinative bonds between metal ions and organic linkers, are metal–organic frameworks (MOFs) and their derivatives. Their reactivity can be further adapted through additional ligands, as shown for acetylacetone anchored onto MIL-125, a Ti-based MOF.[24]

The chemical nature of the ligands plays an essential role in the redox processes taking place at the semiconductor surface; firstly, a ligand that introduces additional states both near the valence band edge and within the gap can contribute to the band-gap reduction and thus facilitate the electronic transition from the valence to the conduction band. Also, ligands with suitable electronic properties are capable of literally ''draining'' the electrons by stabilising them at the surface, where they are ready to react. In addition, the fine molecular structure modification, in terms of electron-donating or electron-withdrawing substituents on a ligand, can modify the electron density around the metal centers, which in turn affects their nucleophilicity and redox potential. The kind of interaction (physical or chemical adsorption and coordination bonding) and its geometry also contribute to determining the electronic coupling in oxide–organic hybrid materials.

In this direction, the ligand-to-metal CT mechanism in TiO_2 photosensitization was investigated by experimental and theoretical methods. For example, several carboxylic acids were found to improve the photoresponse, e^-/h^+ separation, and the overall catalytic efficiency when adsorbed on TiO_2:acetic,[25] oxalic,[26] malonic,[27] terephthalic,[28] *p*-aminobenzoic[29] and salicylic acid[30,31] were employed in visible light driven degradation of organic pollutants, selective oxidation or CO_2 reduction. On the other hand, our previous studies demonstrated that TiO_2–diketone hybrid materials synthesized by a sol–gel technique can spontaneously activate molecular oxygen, producing superoxide radical anions that are preserved by adsorption on their surface.[32,33] The consequent oxidative activity was proven in the removal of various water organic pollutants even in the absence of irradiation.[34,35] A similar unconventional ability was also revealed for resin acid-modified titania particles and employed in polyethylene microplastic degradation.[12]

Following our recent works on CT and stabilization of radical species on TiO_2-based materials with diketones, catechol and resin acid as ligands,[12,31] we have changed our point of view. Our proposal is to study this process starting from the formation mechanism of these materials: the role of the ligand is essential in modulating the morphology and catalytic properties of the material itself. In this way, we hypothesise the behaviour of the organic molecules as ''defectivity controllers'' of the resulting hybrid materials.

Is it possible that the ligand plays an active role in oxygen vacancy formation? Can we expect to predict the activity of a TiO_2 hybrid material by a structural study of the ligand?

Here, an extensive study of TiO_2–organic complexes is conducted through a combination of theoretical and experimental approaches; based on QM and PBC studies the interaction of ligands belonging to different classes of organic compounds with the defective TiO_2 surface is studied to rationalise and evaluate how different functional groups on the same class of compounds affect the geometry, bond energy, charge distribution, electronic states, and the ability to reduce O_2 and generate stabilized superoxide radicals in the air. We present an interesting correlation between the stability of the catalyst precursor [$Ti(OR)_4$ + L] and that of the surface-adsorbed ligand [L + (TiO_2)], which is responsible for the formation and stabilization of oxygen vacancies on the outer surface of the final hybrid material. This approach allows surface charge stabilization, which can readily stabilize chemical species to form reactive intermediates involved in numerous catalytic mechanisms (*e.g.*, reactive oxygen species, ROS). These theoretical predictive results are confirmed by experimental data from the spectroscopic characterization of a series of hybrid TiO_2-based samples synthesized *via* a sol–gel technique. Specifically, NMR spectroscopy attested the formation of Ti^{4+}–L complexes in solution, while FTIR, DRUV-vis, and EPR spectroscopies elucidated the structural, optical and electronic features of the materials.

2. Results and discussion

2.1. QM-DFT calculations: formation steps of hybrid materials

Titanium oxide–organic hybrid materials with peculiar optoelectronic properties and surface reactivity are synthesized by a sol–gel process, which is a bottom-up method, starting from a Ti(IV) alkoxide precursor ($Ti(OR)_4$) and an organic molecule able to act as a ligand (L), preferably bidentate, such as a diketone or a carboxylic acid.[12,35,36] In order to study how the ligand can affect the growth and the formation of the external surface of the final sol–gel material, we performed quantum mechanics (QM) calculations on the first step of the synthesis procedure.

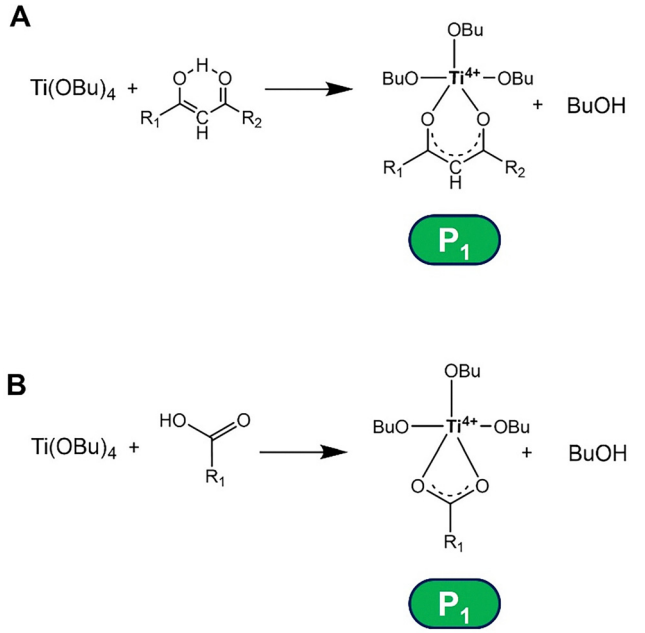

Fig. 1 Reaction between a Ti(IV) alkoxide (titanium(IV) tetrabutoxide) and a generic 1,3-diketone molecule in the enol form (A), or a generic carboxylic acid molecule (B), giving a partially substituted Ti(IV) complex and an alcohol molecule. This reaction leads to a product ($\mathbf{P_1}$) in which the titanium, bonded to the ligand, keeps a 4+ oxidation state.

The assumption is: in the preparation of the hybrid material, $Ti(OR)_4$ reacts with the organic molecules forming partially substituted $Ti(OR)_3L$ complexes, as schematized in Fig. 1. Then, hydrolysis and condensation reactions start the growth of the oxide network, preserving most of the ligand owing to its strong Ti–L coordination bond. The ligands likely located at the surface of the oligomeric aggregates could hinder the formation of an extended TiO_2 lattice, driving the growth of an amorphous gel.[37,38] In addition, the ligand-to-metal charge transfer character of these complexes, with the possible contribution of other suitable reducing agents, such as the alcohol that is both the solvent and a hydrolysis product, results in a mildly reducing environment. Consequently, the final product will show oxygen vacancies and Ti(III) sites in the external surface due to the presence of the ligand,[36,39] as previously ascertained for TiO_2 hybrid gels with coordinated acetylacetone or abietic acid, which exhibited substoichiometry and a small fraction of Ti^{3+} at the surface.[12,36] The more favoured the formation of $Ti(OR)_3L$ ($\mathbf{P_1}$ in Fig. 1), the more favoured the formation of O vacancies or other defects in the external surface and the greater the expected efficiency of the photocatalyst, for example, in the generation of superoxide radicals.[40,41] Accordingly, we calculated the energy involved in the reaction between $Ti(OBu)_4$ and the organic ligand (L) with formation of $\mathbf{P_1}$ and BuOH ($\Delta E_{\mathbf{P_1}}$ and $\Delta G_{\mathbf{P_1}}$ in the solvent, kcal mol^{-1}) as in Fig. 1. For this reaction, the monomeric $Ti(OBu)_4$ precursor and respective ligand represent the zero-energy reference.

We started the calculations considering the organic molecules already used in the synthesis of hybrid sol–gel materials tested in the formation and surface stabilization of ROS, namely β-diketones such as dibenzoylmethane (Hdbm) and acetylacetone (Hacac) and diols such as catechol (H_2cat).[32] A single ligand substitution $Ti(OBu)_3L$ is considered because it is the most probable case when the complexing ratio (L/Ti) is low (it is mainly around 0.2 mol mol^{-1} in the experimentally studied systems). As reported in Table 1 (entries 1–3), the interaction energies of the $\mathbf{P_1}$ complex are thermodynamically favourable in the case of diketonate ligands, dbm and acac, *i.e.*, −10.5 and −10.1 kcal mol^{-1}, respectively. On the other hand, the formation of the $\mathbf{P_1}$ complex when L is catecholate (cat) is unfavoured with an E_{int} of 9.5 kcal mol^{-1}. In these complexes the presence of electron-withdrawing or electron-donor R groups linked to the carbonyl is crucial to increase or decrease the interaction energy, respectively. In the case of catechol, the hybrid formation process becomes energetically unfavourable, as can be seen from the interaction energy becoming endothermic; this can be attributed to a less stable steric situation, *i.e.*, a 5-membered heterocycle, and a lower electronic contribution than diketones. In this case there is an ineffective delocalisation of charge in the binding site, which makes the respective $\mathbf{P_1}$ intermediate unstable, in agreement with previous data reported.[32]

After testing the suitability of this QM method, we moved on to analyse other ligands, starting from diketones with a modified structure, to understand the role of substituent functional groups. In order to evaluate the electronic contribution alone, avoiding the steric influence of the side groups, we made modifications by substituting the methyl groups of acac with electron-withdrawing substituents such as $-CF_3$ and $-NO_2$ and electron-donor groups such as $-OCH_3$ and $-N(CH_3)_2$. Steric maps demonstrating the absence of significant changes brought about by these substitutions are given in the ESI† (Fig. S1). Substitution with electron-attractor groups improves relative stability, while donor groups worsen relative E_{int}–$\mathbf{P_1}$, confirming the results obtained (Table 1, entries 5–8). To extend our data, we examined 2,5-hexanedione, a γ-diketone that demonstrates the importance

Table 1 QM calculation for the complexation reaction leading to the $\mathbf{P_1}$ product

Entry	Ligand	ΔE_{int} $\mathbf{P_1}$[a] (kcal mol^{-1})	$\Delta\Delta E_{int}$ $\mathbf{P_1}$[b] (kcal mol^{-1})	$\Delta\Delta G_{int}$ $\mathbf{P_1}$[c] (kcal mol^{-1})
1	Dibenzoylmethane (Hdbm)	−10.5	0	0
2	Acetylacetone (Hacac)	−10.1	0.5	1.4
3	Catechol (H_2cat)	9.5	20.1	7.2
4	2,5-Hexandione (Hhex)	7.7	18.3	19.6
5	Acac_CF_3	−16.0	−5.5	−4.5
6	Acac_NO_2	−10.0	0.5	1.1
7	Acac_$N(CH_3)_2$	−1.9	8.7	9.3
8	Acac_OCH_3	3.2	13.7	15.4
9	Acetic acid (AcOH)	−3.4	7.1	5.3
10	Trifluoroacetic acid (HTfac)	−5.0	5.5	2.8
11	Benzoic acid (HBz)	−4.3	6.2	4.5

[a] Interaction energy (ΔE_{int}-$\mathbf{P_1}$). [b] Interaction energy compared to the most stable ligand ($\Delta\Delta E_{int}$-$\mathbf{P_1}$). [c] Gibbs free energy compared to the most stable ligand ($\Delta\Delta G_{int}$-$\mathbf{P_1}$).

of charge delocalization in stabilizing the final complex. In this case, E_{int}–$\mathbf{P_1}$ is disfavoured due to the presence of 2 methylene bridges spacing the carbonyl functional groups, a factor that leads to a less stable complexation compared to β-diketones. This effect is related to a folded 7-member binding conformation of the ligand, and a strongly unstable electronic situation.

Then, we turned the attention to carboxylic acids, another class of ligands that has attracted interest in the modification of semiconducting oxides. Their molecular structure, *e.g.* the substituents on the ring of aromatic acids, was shown to have a marked impact on the charge transfer and photoinduced behaviour in TiO_2.[42,43] Therefore, we selected different carboxylate ligands, both monodentate and polydentate, namely acetate (AcO), trifluoroacetate (Tfac), benzoate (Bz), terephthalate (Tpa) and citrate (Cit). This class of ligands have an overall worse stability than diketones because of the formation, in the complexation reaction, of sterically and electronically more unstable 4-membered heterocycles (see Fig. 1(B)). Aligned with the data obtained for diketones, and as shown in Table 1 (entries 9–11), the presence of electron-attracting substituents alpha to the carboxyl functional group resulted in complexes with more stable Ti–L bonds.

Our results, shown in Table 1, indicate that the interaction between the precursor species and the diketone ligands is generally more favoured in terms of energy than that with carboxylic acids, of around 5.5(2.8) kcal mol^{-1} considering the most stable $\mathbf{P_1}$ intermediates of each class (dbm and Tfac in Table 1). In other words, β-diketones lead to thermodynamically more stable Ti(IV) heteroleptic complexes (see $\mathbf{P_1}$ in Fig. 1) that will act as precursors of the hybrid materials. This can be explained by the greater steric and electronic stabilisation of the former class of ligands compared to the latter: in detail, the complexes formed by the diketones consist of a 6-membered heterocycle with larger charge delocalisation, whereas the carboxylic acids form sterically and electronically more unstable 4-membered heterocycles.

Finally, another suitable strategy for improving the efficiency of these complexes in terms of ROS production is through the introduction of ligands that possess multiple chelating groups, as in the case of terephthalic acid (H_2tpa) and citric acid (H_3cit). This peculiar multidentate structure allows the formation of complexes that strongly influence the morphology and electronic properties by inserting themselves into the network of the growing material during the sol–gel process. Our results, shown in Table 2, indicate that in both cases the mono-metallic complex is less stable than the bi-metallic one (entries 2–5). This effect is strongly evidenced in H_3cit, where a tri-metallic complex is also possible (entry 6), showing a non-linear correlation. This structure/activity correlation was experimentally demonstrated by means of EPR spectroscopy (Fig. S2 and S3, ESI†), as a gradual increase in the citrate/$Ti(OBu)_4$ ratio was found to have a non-linear correlation with the density of ROS detected on the samples, confirming such multifaceted behaviour (see Section 2.5). The implications of these theoretical studies suggest some suitable strategies to improve catalytic efficiency. In more detail, the introduction of electron-withdrawing groups in the α-position relative to the functional group, a strong charge delocalisation and the presence of additional chelating groups are valid methods to increase the efficiency of the metal–ligand interaction and the related activity in terms of ROS production.

2.2. Periodic boundary condition (PBC) calculations

PBC calculations were performed to further verify the consistency of the data obtained in QM moving from the calculation of the first reaction steps in solution to the formation of TiO_2-based hybrid materials. We also investigated the structural and electronic features of the hybrid materials. The presence of the local disorder typical of these materials was modelled by removing an oxygen atom from the external layer (VO1) of the stoichiometric anatase (101) surface, in agreement with previous work.[32,44]

In detail, we considered the adsorption of diketones and carboxylic acids in their anionic form. In particular, for the class of diketones, we examined dibenzoylmethanoate (dbm), acetylacetonate (acac) and 2,5-hexanedionate (hex), while for the carboxylic acids, we considered acetate (AcO), trifluoroacetate (Tfac), benzoate (Bz), terephthalate (Tpa), and citrate (Cit). The interaction of phenols with the TiO_2 surface is mostly studied in view of their degradation and it was recently reported that the dissociative adsorption of phenol on the TiO_2 surface brings about a marked electronic coupling and interfacial charge transfer.[45,46] Thus, we also considered phenolate (Ph). Finally, acetic anhydride (Aca) was chosen as a representative of anhydrides, because of its structural similarity to β-diketones.

According to PBC results, all ligands (except for monodentate phenolate) are adsorbed *via* a bidentate coordination mode

Table 2 QM calculation for the complexation reaction leading to the $\mathbf{P_1}$ product for mono-, di- and trimetallic complexes of H_2tpa and H_3cit

Entry	Ligand	ΔE_{int} $\mathbf{P_1}$[a] (kcal mol^{-1})	$\Delta\Delta E_{int}$ $\mathbf{P_1}$[b] (kcal mol^{-1})	$\Delta\Delta G_{int}$ $\mathbf{P_1}$[c] (kcal mol^{-1})
1	Dibenzoylmethane (Hdbm)	−10.5	0	0
2	Terephthalic acid mono-complex (H_2tpa)	−4.1	6.4	4.6
3	Terephthalic acid bi-complex (H_2tpa)	−9.8	0.8	2.7
4	Citric acid mono-complex (H_3cit)	−3.6	6.9	5.3
5	Citric acid bi-complex (H_3cit)	−8.2	2.3	1.1[d]
6	Citric acid tri-complex (H_3cit)	−17.5	−6.9	−0.9[d]

[a] Interaction energy (ΔE_{int}-$\mathbf{P_1}$). [b] Interaction energy compared to the most stable ligand ($\Delta\Delta E_{int}$-$\mathbf{P_1}$). [c] Gibbs free energy compared to the most stable ligand ($\Delta\Delta G_{int}$-$\mathbf{P_1}$). [d] A free energy correction of −3.5 kcal mol^{-1} was applied to avoid an overestimation due to the loss of translational and rotational entropy in solution in the reactions involving a 3-to-1 (or 4-to-1) variation between reactants and products.

through the two O atoms of the functional group bound to the surface site of a sub-coordinate titanium, close to the O-defective site. As a result, the ligands restore a hexa-coordinate configuration of the Ti atom. It is worth noting that their preferred binding mode reflects the coordination predicted for the monomeric complex in solution (see Section 2.1). The optimised geometries of each hybrid system are shown in Fig. 2. The adsorption energies (E_{ads}) for the β-diketonate ligands hex, acac and dbm are −1.64, −2.58 and −2.73 eV, respectively (Fig. 2(A)). These energy values suggest that in β-diketones, the substitution at α to the carbonyl carbons of electron-donor groups, such as R = –CH_3 in acac and hex, with electron-withdrawing groups, such as phenyl in dbm, causes an increase in the adsorption energy. This has been attributed to a different electronic behaviour of the C═O bond, where the electron withdrawing groups make carbonyl carbon less charged, while oxygen has a higher nucleophilic character allowing it an easier bond formation with the surface titanium atom (see Bader charges in Table S1, ESI†). Moving to analyse the E_{ads} of carboxylic acid ligands, we report for AcO, Tpa, Tfac, Bz, and Cit the following values: −0.44, −1.63, −1.71, −1.96 and −2.15 eV, respectively (Fig. 2(B)). When comparing the E_{ads} of AcO with Tfac, it is clear that the latter interacts with the surface in a more stable manner due to the strong inductive effect of the fluorine atoms, which modify the charge distribution in the complex, polarising the C═O bond similarly to what described above in the case of diketones (see Table S1, ESI†). Another interesting comparison is that of Tpa with Bz (see Fig. 2(B)). Despite the very similar chemical structure, in the former there is a negative contribution to coordination by the carboxylic group in the *para* position, which could indirectly exert an inductive electron-attracting effect, softening the electron-withdrawing effect of the aromatic ring. In addition, Cit shows the best adsorption energy among carboxylate ligands. In this case, the coordination to the surface is highly favoured due to the contribution arising from the formation of an H-bond with a surface oxygen atom. The E_{ads} values of the other studied compounds are −1.30 for Aca and −1.61 for Ph (Fig. 2(C)). Despite the presence of two chelating oxygens, Aca binds weakly to the surface due to its neutral character, while Ph adsorbed in its anionic form has a low interaction energy, due to the presence of only one oxygen binding to the two sub-coordinated Ti atoms.

We calculated also the formation energy for the oxygen vacancy based on the most energetically favourable position, VO1. The results are 1.64, 1.90 and 3.01 eV for dbm, acac and

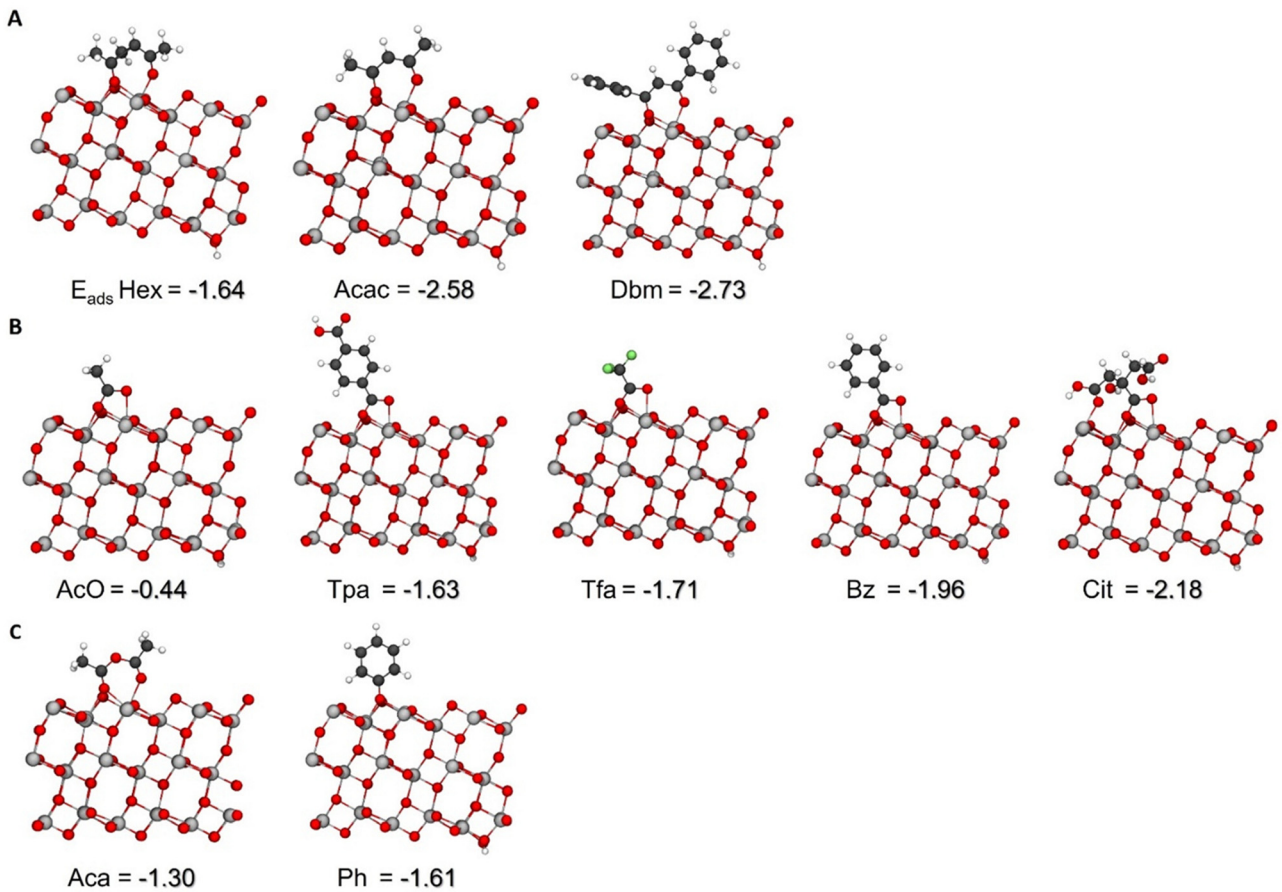

Fig. 2 Optimized structure of the interaction of the TiO_2 (101) surface containing oxygen vacancy VO1 with diketones (A), carboxylic acids (B) and other classes of ligands (C) and the corresponding adsorption energies (E_{ads}, eV). Ti, C, H, O and F atoms are represented in ball and sticks and depicted in gray, dark gray, white, red and green respectively.

hex, and 2.89, 2.88, 2.77, 2.68 and 2.17 eV for AcO, Tfac, Bz, Tpa, and Cit, respectively. An interesting correlation is observed between the energies associated with ligand adsorption and O vacancy formation: the ligands whose interaction with the TiO_2 surface is more exothermic generally have a higher tendency to promote and stabilize a nearby vacancy.

In addition, a detailed analysis of the spin density and projected density of states (PDOS) was carried out on all considered systems (see Fig. S4–S6, ESI†), supplemented by an examination of the frontier molecular orbitals to gain further insight into the electronic structure (see Fig. S7 and S8, ESI†).[47] Our results suggest that the formation of an oxygen vacancy leaves an excess of two electrons within the surface that is located on the d orbitals of Ti near the vacancy site, generating Ti^{3+}, as previously reported.[32,48] The PDOS plots of the lowest energy configurations with ligands coordinated to the anatase TiO_2 (101) surface, in the presence of VO1 vacancy, show that the coordination of organic ligands contributes to reducing the band gap compared to the pure anatase (an experimental gap of 3.2–3.3 eV[15] and a theoretical gap of 3.0 eV).[32] For all these materials, the valence bands (VB) have mainly O 2s and 2p characters and the conduction band (CB) displays a Ti 3d character.

Moving on to study the catalytic efficiency in the formation of ROS on the different systems, we note that all hybrid materials, regardless of the ligand considered, are active in the production of superoxide radicals by reduction of adsorbed O_2. The adsorption of O_2 at high coverage, which best reproduces the experimental conditions,[32] was also investigated for the various ligands and the optimised structures with their respective E_{ads} are reported in the ESI.† From the study of catalytic efficiency, assessed in the O_2 adsorption and reduction at high coverage, we were not able to show considerable quantitative differences in ROS formation among the different systems, probably due to the inherent limitations of the model. Since the presence of several chelating groups can lead to the formation of different coordination modes, our idea is that this feature can result in hybrid materials with increased catalytic activity due to the strong influence of the ligand in the growth stages of the material. This leads to an extremely varied morphology in terms of defects and quantitative surface distribution of vacancies. In this way, the ligand acts as a defectivity controller in the resulting material, increasing the number of surface O vacancies, the Ti^{3+}/Ti^{4+} ratio and, consequently, the sites for O_2 adsorption. In fact, ligands such as citrate (as shown in Fig. S9, ESI†), due to the presence of multiple chelating groups (carboxyl and hydroxyl), can interact in different ways with the precursor species, thus modulating, during the growth of the hybrid material, the formation of O defects in its structure and eventually the production of ROS.

2.3. Selection of TiO_2–organic systems for the experimental study

Following the results of the computational investigation, a series of TiO_2–organic hybrid materials were synthesized in order to connect the theoretical predictions with experimental evidence. The functional group directly involved in the interaction with the metal oxide surface plays a central role in determining the features of the complex and its influence on the surface reactivity, as suggested by our recent report on TiO_2 modified with β-diketones (Hacac and Hdbm) as well as catechol.[32] Previous results showed that the ability of TiO_2–diketonate hybrids to generate and stabilize ROS translates into a significant oxidative degradation activity.[34–36] Bidentate enediol ligands such as catechol and ascorbic acid have been extensively studied in combination with TiO_2, proving effective photosensitization in the visible light range due to charge injection.[22,49] However, based on our previous spectroscopic characterization, they appear unable to stabilize oxygen radicals, which was suggested by DFT modelling to depend on the more widespread distribution of electron density through the oxide surface.[32,50] Therefore, we did not further examine enediols in this experimental work. Phenol was not included either, as it gives a rather weak monodentate coordination with surface Ti ions, which is unfavourable for the chemical stability of a hybrid material. Acetic anhydride was excluded as well because of its instability in the presence of water. We chose carboxylic acids for further exploration of TiO_2-based hybrids, because of their ubiquity and availability, the promising modelling results about their complexation, and preliminary EPR data revealing their ability to promote the formation of superoxide radicals on the TiO_2 surface[12] (see also Section 2.5). All the organic acids included in the theoretical studies were considered, so as to compare a linear ligand such as acetate, an analogue with a strongly electron-withdrawing group (trifluoroacetate), aromatic mono- (benzoate) and dicarboxylate (terephthalate) and a tricarboxylate (citrate).

The materials were prepared through the sol–gel method, starting from $Ti(OBu)_4$, as described in Section 3.2. By this approach, previously adopted for the synthesis of TiO_2 gels with diketones and diols,[36,50] metal complexes are formed in solution before hydrolysis and condensation reactions. A relatively low complexing ratio (0.2 mol mol^{-1}) was chosen in order to obtain materials with a part of Ti ions in the oxide matrix involved in coordination complexes. High complexing ratios may hinder the growth of uniform oxide networks, result in an incomplete incorporation of the ligand in the final structure, or cause saturation of the surface, thus lowering the availability of active sites for the adsorption of O_2 and target molecules. To gain insight into this first stage of the synthesis, NMR spectroscopy was employed, while FTIR, DRUV-vis and EPR spectroscopies were used for the characterization of the products.

2.4. NMR study of Ti^{4+} complexation

The modification of Ti alkoxides by organic ligands is a common way to enable a better control of the sol–gel growth of titanium-based solids and obtain hybrid gels with specific physicochemical and morphological properties.[51] The complexation of $Ti(OR)_4$ compounds with polydentate ligands can be studied through ^{13}C, ^{1}H NMR and FTIR spectroscopy.[52–54] Since this is a crucial step in the synthesis procedure, here NMR spectroscopy was used to verify the interaction of a representative carboxylate and a

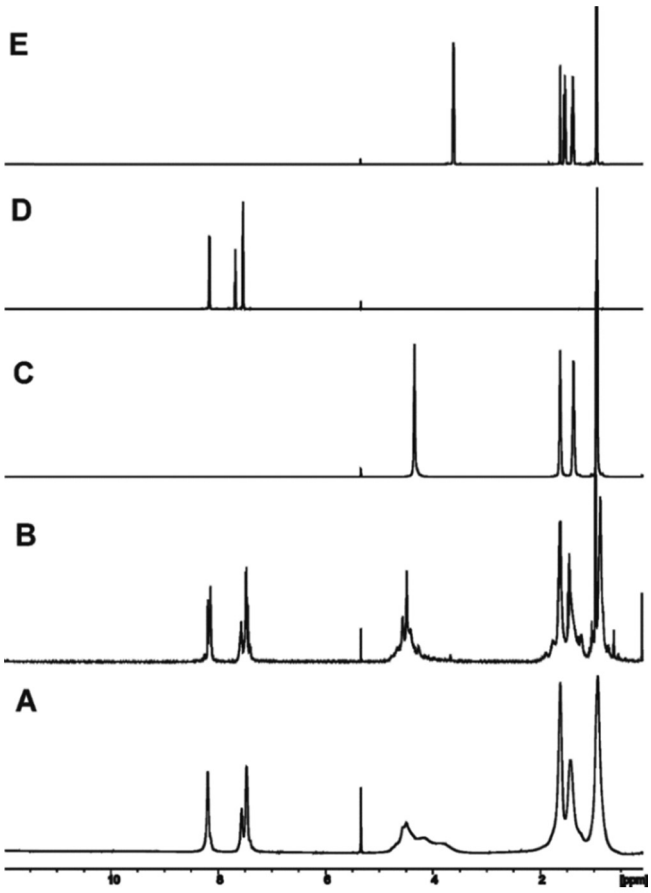

Fig. 3 ^{1}H NMR spectra (CD_2Cl_2, RT, 600 MHz) of $Ti(OBu^n)_4$: HBa 1 : 1 reaction mixture (A); $Ti(OBu^n)_4$: HBz 1 : 1 after removal of butanol (B); $Ti(OBu^n)_4$ (C); HBz (D); and butanol (E).

diketonate ligand with $Ti(OBu^n)_4$. First, we examined benzoic acid, which has not been widely investigated in this scope to date.[55] Both ^{1}H and ^{13}C NMR spectra of the $Ti(OBu^n)_4$: HBz system in a 1 : 1 molar ratio were compared with those of CD_2Cl_2 solutions of pure reactants and butanol. The ^{1}H NMR spectra are shown in Fig. 3. As can be seen, the proton signals of benzoate groups (Fig. 3(A)) are slightly shifted with respect to those of pure HBz (Fig. 3(D)), specifically aromatic resonances are at δ = 8.19 ppm (*ortho*-CH), 7.47 ppm (*meta*-CH), and 7.56 ppm (*para*-CH) for the complex, and at 8.16 ppm (*ortho*-CH), 7.68 ppm (*meta*-CH), and 7.54 ppm (*para*-CH) for the pure acid, suggesting that Bz is coordinated to titanium. The broad signals in the region where the $-H_2C-O$ butoxy group resonances are expected (3.80–4.80 ppm) are attributable to the $-H_2C-O$ groups bonded to the titanium center, along with those of released butanol in the solution. It is not possible to differentiate them because they are too close and partially overlapped with each other. The broadness of these resonances suggests that OBu^n ligands are in different environments (*e.g.*, terminal and bridging positions) and in a rather slow exchange with released butanol.[52] It should be considered that $Ti(OR)_4$ compounds containing primary alkoxide groups (OEt, OPr^n, and OBu^n) typically form trimers with pentacoordinated titanium centers in the liquid phase and alcohol solution, due to steric hindrance.[56]

^{1}H NMR resonances corresponding to free benzoic acid (the COOH proton signal at around 12 ppm) are not observed in the reaction mixture. This indicates that all HBz is virtually bonded to titanium. The formation of esters could occur through condensation of free HBz with BuOH, or through transesterification between coordinated and free ligands;[51,57] however no signals for butyl benzoate are detected. The ^{1}H NMR spectrum of the $Ti(OBu^n)_4$: HBz system after vacuum treatment (Fig. 3(B)) confirms the removal of butanol from the reaction mixture. The integration of the area of the NMR signals of the butoxy and Bz groups shows a molar ratio of 3 : 1, clearly indicating that the reaction between benzoic acid and $Ti(OBu^n)_4$ proceeds with the substitution of one butoxy group by a benzoate one, as in eqn (1), with consequent release of BuOH in solution, leaving no free HBz in solution:

$$Ti(OBu^n)_4 + C_6H_5COOH \rightleftarrows Ti(OBu^n)_3(OOCC_6H_5) + Bu^nOH \quad (1)$$

The ^{13}C NMR analysis (Fig. S10, ESI†) also supports the above findings. The spectrum of the reaction mixture displays the carbon atom of the carboxylic group as a very broad peak centered at 172.7 ppm and the aromatic CH signals at 132.8 ppm (*para*-CH), 130.8 ppm (*ortho*-CH), 128.9 ppm (*C*-COOH), and 128.7 ppm (*meta*-CH), whereas the ^{13}C NMR spectrum of HBz shows resonances at δ = 173.3 ppm (COOH), 134.6 ppm (*para*-CH), 130.8 ppm (*ortho*-CH), 130.0 ppm (*C*-COOH), and 129.3 ppm (*meta*-CH). From the comparison with the spectrum of $Ti(OBu^n)_4$, in the region where resonances of the $O-CH_2$ butoxy groups are expected, two broad bands can be observed at 77.2 and 64.0 ppm. They can be associated with $-H_2C-O$ groups bonded to the titanium center and H_2C-O groups of released butanol, respectively. The broadness of the diagnostic resonances associated with the formation of the metal complex could be related to different chemical environments that surround the carbon atoms bonded to titanium, including the possibility of benzoate groups acting as monodentate or bidentate ligands. The removal of butanol from the reaction mixture results in sharper resonances for the $Ti(OBu^n)_4$:HBz system, still consistent with a varied environment for the bonded groups. Although from the present NMR study it is not possible to describe in detail the nature of the bonding between the benzoate groups and Ti; in analogy with previous works on the complexation reaction of Ti(IV) monomers and oligomers with carboxylic acids, it is reasonable to assume that the benzoate groups bonded to titanium behave preferentially as a bidentate ligand.[54,58]

Turning to β-diketones, they are known to act as chelating ligands and give at most disubstitution on Ti(IV) alkoxides for steric reasons. In solution, an equilibrium between monomeric $Ti(OR)_3$(diketonate) and dimeric species can appear, depending on the OR group.[59,60] The reaction of $Ti(OBu^n)_4$ with dibenzoylmethane was examined, as most previous studies dealt with Hacac and no data about this reaction have been found in the

literature. The ^{1}H NMR spectra of the equimolar mixture of $Ti(OBu^{n})_4$ and Hdbm, compared with those of CD_2Cl_2 solutions of pure reactants and butanol, are shown in Fig. S11 (ESI†). In brief, the spectrum of the reaction mixture (Fig. S11A, ESI†) shows several peaks in the region of Hdbm that are shifted with respect to those of the pure compound (Fig. S11D, ESI†), particularly three peaks attributable to the CH protons about 7.00 ppm. The ^{13}C NMR spectrum of the $Ti(OBu^{n})_4$:Hdbm system (Fig. S12, ESI†) is in good agreement with the ^{1}H NMR spectrum. Three peaks are detected in the CH region at 95.6, 95.7 and 96.7 ppm, shifted with respect to that of the pure ligand (δ = 93.8 ppm). Moreover, three carbonyl carbon resonances at 185.6, 184.0, 182.8 ppm can be observed, while the CO carbon atom of pure Hdbm shows only one resonance at 186.5 ppm. The presence of different O–CH_2 butoxy groups also indicates an equilibrium between several species in solution. The proton spectrum after solvent removal (Fig. S11B, ESI†) confirms the presence of 3 butoxy groups per β-diketonate group and highlights a change in the ratio between the CH resonances. In line with previous reports on the reaction of $Ti(OEt)_4$ with Hacac,[59,60] it is reasonable to hypothesize an equilibrium in solution between monomeric $Ti(OBu^{n})_3$(dbm) and dimeric species in which titanium is surrounded by one dbm ligand and two terminal and two bridging butoxy groups. For more details on the peak assignment see Table S4 (ESI†).

2.5. Spectroscopic study of TiO_2–organic hybrids

The persistence of the coordinative bonding in the gel-derived solids was ascertained by FTIR spectroscopy, while electron paramagnetic resonance (EPR) spectroscopy was employed to inspect the presence of radical species in the samples. All the FTIR spectra of hybrid samples containing carboxylate ligands (see Fig. 4(A) and Fig. S13, ESI† for the full frequency range) show a large shift of the characteristic carbonyl stretching band from above 1700 cm^{-1} (in the pure organic acids) to lower wavenumbers, attesting the complexation of titanium. The infrared spectra of metal–carboxylate complexes are generally characterized by two major bands corresponding to the asymmetric and symmetric stretching of the carboxylate group, and the separation between these bands is considered indicative of the coordination geometry (monodentate, bridging or chelating). In the T–Ac sample these two bands appear centred respectively around 1531 and 1435 cm^{-1}, the latter being split into two components. The separation, about 90 cm^{-1}, is consistent with a bidentate chelating mode, in good agreement with studies on acetic acid adsorption on TiO_2 powder[61] and on the modification of Ti alkoxides with acetic acid,[57,62,63] which suggested both chelating and bidentate complexes as possible intermediates, with the former being more stable under hydrolytic conditions and thus more likely preserved in the oxide structure. The structure of the synthesized hybrid materials is amorphous (X-ray diffraction patterns not shown), as usually found for titanium oxides derived from a low-temperature sol–gel process. Although an amorphous structure is generally considered unfavourable for the photoelectric properties, amorphous titania has shown interesting performances in photocatalysis and electronics (*e.g.*, thin film transistors), related to the energy states near the band edges derived from the disordered atomic arrangement.[64,65]

EPR measurements were performed at room temperature in the dark in order to evaluate the formation of oxygen radicals without pre-treatments or external stimuli, such as light irradiation. The reference amorphous titania powder synthesized by a sol–gel process gives no paramagnetic signal (Fig. S2, ESI†),

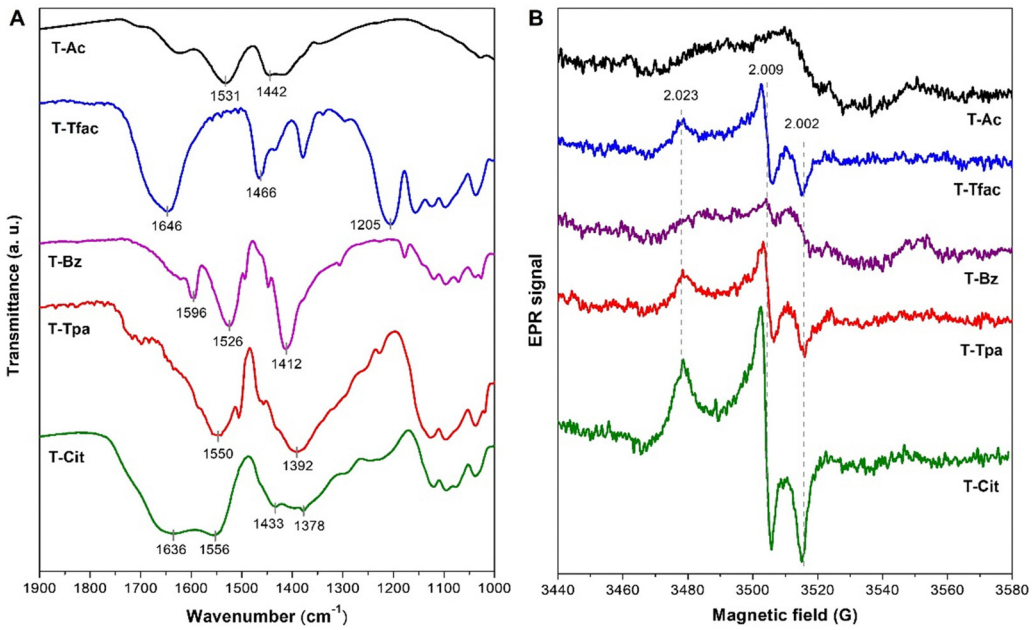

Fig. 4 FTIR spectra (A) and EPR spectra, recorded in air at room temperature, in the dark (B), of the studied TiO_2–carboxylate samples with the ligand/Ti molar ratio = 0.2 (*g* values of the EPR signals are indicated).

as previously reported,[36] indicating the absence of detectable radical species. The EPR spectrum of T–Ac (Fig. 4(B)) shows a weak undefined signal. However, the analysis of a sample prepared using a higher concentration of acetic acid (Ac/Ti equimolar ratio) to check if the ligand concentration affects the surface activity revealed the typical anisotropic signal of the superoxide radical anion adsorbed on the TiO_2 surface[40,66] (Fig. S2, ESI†). The ability of the coordination complex to induce the spontaneous formation of superoxide by reduction of atmospheric O_2 and its immobilization on the surface in the absence of continuous photoexcitation attests intrinsic redox properties. These were previously observed for TiO_2-based hybrids with diketone and abietic acid as ligands, which have significant degradation activity toward different organic pollutants in water (phenanthrene, 2,4-dichlorophenol, chlorinated phenoxy herbicides, methylene blue, and even polyethylene microplastics).[34–36,67] The ROS-mediated mechanisms initiated by these materials in an aqueous environment can involve $^{\bullet}OH$ radicals, as previously found by EPR spin trapping tests.[34,67] Such oxidative activity, assessed under dark conditions, is likely emphasised under irradiation, as reported in the case of TiO_2–dbm samples.[33] The evidence collected for TiO_2–acetate drove the experimental investigation of hybrids containing other carboxylate ligands.

In the T–Tfac sample, the FTIR bands assigned to asymmetric and symmetric stretching of COO^- are observed at 1646 and 1466 cm^{-1} (Fig. 4(A)), close to previously reported values,[68] with separation (180 cm^{-1}) consistent with bidentate coordination, while the bands at 1205 cm^{-1} and lower wavenumbers are attributed to C–F stretching. For T–Bz, the two main carboxylate stretching bands are found at 1526 and 1412 cm^{-1}, in good agreement with predicted and measured values for the molecule adsorbed on TiO_2,[43] the minor bands being mainly associated with vibrations of the aromatic ring. Conversely, for T–Tpa the two bands appear broadened and more distanced (1550 and 1392 cm^{-1}). The comparison of these FTIR spectra with those of pure benzoic and terephthalic acids (Fig. S13, ESI†) shows the shifts of the abovesaid stretching bands. Noticeably, T–Tpa shows only a weak trace of the initial C=O band (around 1685 cm^{-1}), suggesting that both carboxylic groups are involved in interactions with metal ions. The same can be argued for the T–Cit sample, whose situation is more intricate. This hybrid xerogel shows the overlapping of a few features that can be assigned to bonded carboxylate groups, namely those at 1636, 1556, 1433, 1398 and 1378 cm^{-1} (pure citric acid shown in Fig. S13, ESI†). In particular, the bands between 1556 and 1398 cm^{-1} have similar wavenumbers to those attributed to the asymmetric and symmetric stretching of coordinated COO^- in citrate either adsorbed on a TiO_2 surface[69] or added to a $TiCl_4$ solution.[70] The splitting equal to or higher than 123 cm^{-1} suggests a varied scenario, with a range of binding modes, including bridging bonds, and some carboxylate groups which remained free or weakly bound, for example through hydrogen bonds, as confirmed by DFT calculations (see ESI,† Fig. S9).

The EPR results proved the redox behaviour induced by all studied carboxylic acids, as they produced the same characteristic signal of the superoxide radical (Fig. 4(B)). This outcome agrees with the theoretical prediction of surface reactivity in contact with O_2 (see Section 2.2). The different intensities of the signals reflect the variable number of radical species per mass of the sample (radical density), which is around the order of 10^{15} g^{-1}, and follows the trend T–Cit > T–Tfac > T–Tpa > T–Bz (Table 3). The highest density of adsorbed superoxide shown by T–Cit is likely related to the additional carboxylic groups, able to contribute to Ti ion coordination or acting as electron-withdrawing substituents. Indeed, trifluoroacetate is clearly more effective than acetate in generating stable superoxide radicals, which may be attributed to the strong inductive effect of the fluorine atoms, changing the charge distribution in the complex and limiting charge delocalization throughout the oxide surface. A weaker inductive effect coupled with resonance may occur in T–Bz, providing it with a slight ROS-generating activity. For comparison, in β-diketones the replacement of the two methyl groups adjacent to carbonyls in Hacac with two aromatic rings (Hdbm) caused an increase of the estimated radical density of one order of magnitude.[32] In the case of terephthalate, the carboxylic group at the *para* position could indirectly exert again an inductive effect, although its likely contribution to coordination might be the primary factor responsible for the higher O_2 reduction activity with respect to benzoate.

Noticeably, a correlation seems to exist between the surface redox activity of the TiO_2–carboxylate hybrids and the interaction energies for complex formation, evaluated by QM calculations (Tables 1 and 2). Fig. S14 (ESI†) shows that the complexes associated with a higher interaction energy (ΔE_{int}-$\mathbf{P_1}$) tend to stabilize a higher number of radicals on the surface, with an acceptable linearity. Conversely, the adsorption energies on a defective anatase (101) surface, the most favoured adsorption mode (Fig. 2), do not give a satisfactory linear trend with the radical density, suggesting that the QM results are more effective in predicting the materials' reactivity.

The dependence of the radical density on the concentration of ligand, observed using acetate, was assessed also with citrate. Upon increasing the nominal Cit/Ti molar ratio from 0.2 to 0.5 a significant increase of the EPR signal intensity was recorded (with estimated density approaching the order of 10^{17} g^{-1}, see Fig. S3, ESI†), indicating a non-linear positive trend. Besides the electronic features of the complexes, which seem to play a central role in defining the efficiency in the O_2

Table 3 Density of radical centers evaluated from double integration of EPR spectra and energy at the absorption band onset evaluated from DRUV-vis spectra for the analysed TiO_2–carboxylate samples with the ligand/Ti molar ratio = 0.2

Sample	Radical density $\times 10^{-14}$ (g^{-1}) (±10%)	Absorption band onset (eV ±0.1)
T–Ac	—	2.6
T–Tfac	9	2.3
T–Bz	3	2.5
T–Tpa	6	2.3
T–Cit	20	2.3

reduction and stabilization, it cannot be excluded that the different molecular properties of the ligands (polarity and reactivity) affect the surface morphology of the hybrid oxide and thus the availability of adsorption sites.

Interestingly, the g factors reveal a difference between these EPR signals and those recorded for TiO_2–acac and TiO_2–dbm systems:[32] the g_{zz} value, corresponding to the component at a lower field, is slightly shifted from 2.025 to 2.023 in the carboxylate samples. This component is sensitive to the coordinative environment, particularly to the electric field experienced by the anion: a lower g_{zz} value is given by either a higher charge/radius ratio of the metal cation or its lower coordination.[71] In previous works, two or three overlapped signals of superoxide anions located on different sites of the same material are reported, with g_{zz} values ranging between 2.019 and 2.029, assigned to radicals adsorbed on a vacancy site or on under-coordinated Ti^{4+} ions.[66,72] The vacancy sites should correspond to a g_{zz} of about 2.019, lower than the values found here. The dependence of g_{zz} on the type of organic ligand suggests that the adsorption site of superoxide is in close proximity to the coordinated Ti atom. An effect of the coordination mode could be inferred, since compared to chelating β-diketonates, which form a 6-membered ring, the bidentate carboxylate complexes are supposed to fill less efficiently the hexa-coordination of Ti atoms, which agrees with a slightly higher electric field exerted on the near adsorbed superoxide anion.

Another difference between carboxylate and diketonate ligands is the apparent stability over time of the generated superoxide: while TiO_2 hybrids with acac or dbm showed the capability to preserve the radicals for several months or even years under ambient conditions,[32,34] some of the TiO_2–carboxylate samples revealed a substantial decrease in the EPR signal intensity after 3 months of storage (data not shown). This could be explained by a different proneness of the ligand to self-oxidation, even though no evident EPR signals attributed to organic radicals were detected and carboxylate molecules are expected to be relatively stable to oxidation. It is worth mentioning that the lifetime of superoxide anions on the titania surface was reported to be related to the adsorption sites, and those adsorbed on sites giving lower g_{zz} values were observed to have lower thermal and photo-stability, linked to their higher reactivity.[72] Moreover, Ti–Cit complexes in hybrid thin films showed a higher lability than Ti–acac and Ti–dbm ones under UV irradiation,[73] which could hint at easier self-degradation also under ambient conditions.

Experimental information about the electronic structure of the hybrid materials was obtained from UV-visible diffuse reflectance (DRUV-vis) spectra (Fig. 5(A)). The main absorption band, corresponding to the valence-conduction band transition, is not significantly modified in TiO_2–carboxylate samples compared with bare amorphous titania and the absorption edges do not appear largely shifted, as confirmed by the corresponding Tauc plot of indirect transitions (Fig. 5(B)). The band gap values estimated by the intercept of the tangent to the linear part of the curves (drawn in the graphic only for reference titania) are around 3.2–3.3 eV for all the materials, which are typical values for amorphous TiO_2. On the other hand, the band tails generated by electron states near the band edges are emphasized and more pronounced in the hybrid samples than in reference TiO_2, reaching about 500 nm. As the organic ligands do not absorb in the visible range, this can be attributed to a distribution of states introduced by the ligand that cause intragap transitions (see DOS plots, Fig. S4 and S6, ESI†). Similar absorption curve shapes were reported for crystalline titanium oxides modified with benzoate[43] and terephthalate.[74] Based on DFT studies on anatase and rutile TiO_2 clusters functionalized with benzoic acid and derivatives, Fujisawa *et al.* assigned a series of weak excitations in the visible range to interfacial charge transfer transitions from the HOMO of the ligand to the conduction band.[43,75] This interpretation well agrees with the computational data and absorption spectra shown here, suggesting a similar optical behaviour of amorphous and crystalline TiO_2 in the presence of CT complexes, despite the variations in electronic structure between different

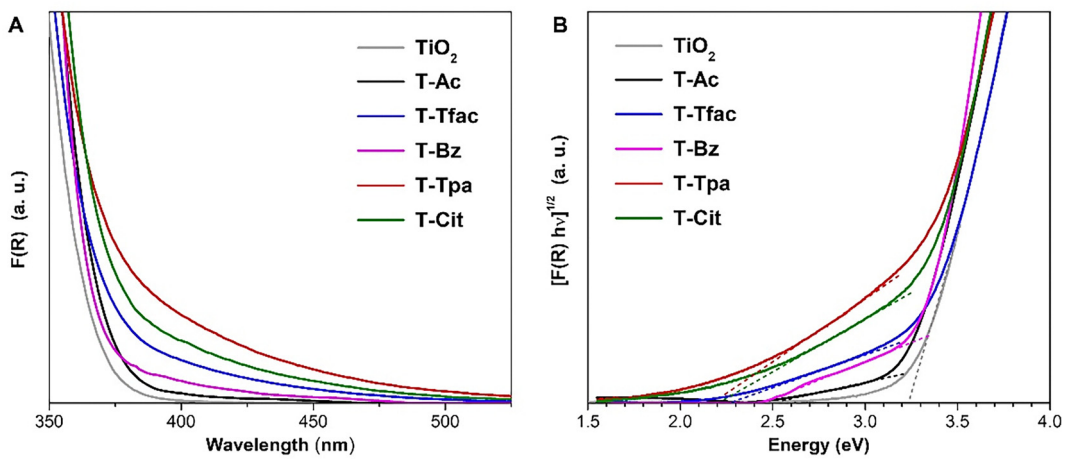

Fig. 5 DRUV-vis spectra of the studied TiO_2–carboxylate samples with the ligand/Ti molar ratio = 0.2 and reference sol–gel TiO_2 (magnification of the normalized Kubelka–Munk function of reflectance, (A)); corresponding Tauc plot for indirect band gap transitions (B).

polymorphs and the disordered oxide. The onset of the side bands in the DRUV-vis spectra can be considered indicative of the apparent (or effective) band gap of the hybrid systems. A fair agreement is found between these approximate onset values, extrapolated from the nearly linear section of the side band (Fig. 5(B) and Table 3) and the gap energy values calculated by DFT, with discrepancies between 0 and 0.3 eV (see Table S2, ESI†).

Though the visible light absorption component related to the carboxylate ligands is generally less intense than that observed for diketonates and less extended than those shown by catechol and other enediols,[32,50] enhanced visible-light-driven photocatalytic performances were reported also for carboxylate-modified TiO_2, for example with acetate,[25] oxalate[26] or terephthalate.[28] The oxidative performances of TiO_2–diketonate hybrids were proven under dark conditions; however, the influence of light cannot be neglected, as it may supplement the effect of interfacial CT.[33] A preceding light exposure is likely to contribute to the storage of charges, which are later used in the absence of irradiation, as occurs in the "memory photocatalysis" or "dark photocatalysis".[76] Under irradiation, besides the direct gap photoexcitation by UV radiation, visible light absorption by the CT complex could synergistically promote surface reactivity. Looking at Fig. 5 and Table 2, it can be noticed that the samples with a more intense and red-shifted absorption side band, namely those with polycarboxylate (T–Tpa and T–Cit) or fluorinated (T–Tfac) ligands, show a higher intensity of the EPR signal. Hence, the ROS stabilization ability could be favoured by molecules forming a higher density of CT complexes with effective charge distribution and enhanced visible light absorption. Further investigation about the effect of light intensity and wavelength on the redox performances of such hybrid semiconductors would unveil more details on the mechanisms of ROS formation, regeneration and action in operating conditions, also under weak or intermittent illumination.

3. Materials and methods

3.1. Computational details

This work adopts a dual approach to describe the complex mechanisms that, starting from complexation reactions in solution, ultimately lead to the formation of the catalytically active species—namely, TiO_2-based hybrid materials—and to understand how these initial complexation reactions influence the properties of the resulting sol–gel material. To this end, two different computational methods were employed:

QM calculations in solution were carried out using the Gaussian 16 program.[77] The B3LYP functional[78] was used to perform the geometry optimizations of all minima in the gas phase, with "normal" convergence criteria (maximum force $<4.5 \times 10^{-4}$ Hartree Bohr^{-1}, RMS force $<3.0 \times 10^{-4}$ Hartree Bohr^{-1}, maximum displacement $<1.8 \times 10^{-3}$ Bohr, and RMS displacement $<1.2 \times 10^{-3}$ Bohr). The LanL2DZ basis set with associate effective core potentials (ECP) was used for Ti and the 6-31G(d,p) basis set[79] for C, H, O, N and F atoms. The reported Gibbs free energies have been obtained adding thermal corrections in gas phase to the electronic energy in solvent (PCM model[80]) computed *via* single point energy calculations in a mixture of water/1-propanol in a 1 : 2 molar ratio (as the experimental condition) at the M06 level.[81] The Triple-z basis set of Ahlrichs (def2TZVP)[82] was used for C, H, O, N and F atoms, while an ECP was employed for Ti. Finally, in Table 2, a free energy correction of -3.5 kcal mol^{-1} was applied to avoid an overestimation due to the loss of translational and rotational entropy in solution in the reactions involving a 3-to-1 (or 4-to-1) variation between reactants and products according to the "free volume theory".[83,84]

PBC calculations were performed using the Quantum-ESPRESSO computer package.[85] The exchange and correlation energy functional expressed in the Perdew–Burke–Ernzerhof (PBE) generalized gradient approximation (GGA)[86] was employed.

The spin-polarized Kohn–Sham equations were solved in the plane-wave pseudopotential framework, with the wavefunction basis set and the Fourier representation of the charge density being limited by kinetic cutoffs of 25 and 250 Ry, respectively. The Ti, O, C, N, F and H atoms were described using ultrasoft pseudopotentials.[87] Self-consistency was considered achieved when the total energy difference between two consecutive iterations was below 1×10^{-7} Ry.

For PBC calculations, we have used a DFT+U approach with a value of U = 3.9 eV, in line with previous studies,[32,44,88] demonstrating that the addition of a Hubbard U term acting on the Ti 3d orbitals allows for a more accurate description of the electronic structure of titanium surfaces.

For more details related to the models and experimental sections, see our previous work.[32]

3.2. Synthesis of the hybrid materials

TiO_2–acetate (T–Ac), TiO_2–trifluoroacetate (T–Tfac), TiO_2–benzoate (T–Bz), TiO_2–terephtalate (T–Tpa) and TiO_2–citrate (T–Cit) samples were prepared by a hydrolytic sol–gel route, using titanium(IV) *n*-butoxide ($Ti(OBu^n)_4$, 97%), acetic acid (99.0+%), trifluoroacetic acid (99%), benzoic acid (99.0+%), terephthalic acid (benzene-1,4-dicarboxylic acid, 98%), citric acid (99%), and ethanol (EtOH, 99.8+%), all purchased from Sigma-Aldrich and used as received. In a typical procedure, a solution of $Ti(OBu^n)_4$, organic ligand (L) and ethanol was prepared under stirring at room temperature. After 30 min, a hydrolytic solution, containing distilled water and EtOH (1 : 1 v/v), was added to the first one. The final molar ratios were $Ti : L : H_2O : EtOH = 1 : 0.2 : 2 : 15$. The solution was kept under stirring until a gel (either chemical or physical) formed, and then the product was aged for 1 day and finally dried at 50 °C in an air-ventilated oven until the weight was constant. The obtained xerogels were ground in a mortar prior to characterization. Some T–Ac and T–Cit samples were prepared with L/Ti molar ratios higher than 0.2, as specified in the text. A bare TiO_2 sample was synthesized as reference by an analogous sol–gel procedure, without adding any organic ligand.

3.3. Spectroscopic characterization

Nuclear magnetic resonance (NMR) spectroscopy was carried out on a BRUKER ASCEND 600 spectrometer (600 MHz for

^{1}H; 150 MHz for ^{13}C) operating at 298 K. The samples for measurements were prepared in a glovebox using NMR tubes equipped with a J. Young valve (Wilmad 528-QPV-8) and deuterated dichloromethane (CD_2Cl_2) as solvent. The δ-scale is referenced to residual CH_2Cl_2 in CD_2Cl_2 as internal standard. Further details about the NMR experiments are reported in the ESI.†

The chemical structure of the TiO_2–carboxylate samples was studied by Fourier Transform Infrared (FTIR) spectroscopy using a Nicolet Instrument Nexus model (Thermo Scientific, Waltham, MA, USA) equipped with a DTGS KBr (deuterated triglycine sulfate with the potassium bromide window) detector. FTIR spectra were recorded in the 4000–400 cm^{-1} range at a resolution of 2 cm^{-1} on pressed disks of powders diluted in KBr (1 wt%) and corrected based on blank KBr.

The powder samples were analysed by electron paramagnetic resonance (EPR) spectroscopy employing an X-band (9 GHz) Bruker Elexys E-500 spectrometer (Bruker, Rheinstetten, Germany). The measurements were performed at room temperature, collecting 16 scans, with the following instrumental settings: sweep width, 140 G; resolution, 1024 points; modulation frequency, 100 kHz; modulation amplitude, 1.0 G; time constant, 20.5 ms; attenuation, 10 dB. The *g*-factor values and radical densities were evaluated using an internal standard, Mn^{2+}-doped MgO, calibrated with reference to a diphenylpicrylhydrazyl (DPPH) standard solution.

The optical properties of the hybrid samples were investigated by diffuse-reflectance UV-visible (DRUV-vis) measurements with a UV-2600i UV-vis spectrophotometer (Shimadzu, Milan, Italy), equipped with an integrating sphere ISR-2600Plus, in a wavelength range of 200–800 nm, using barium sulfate as a reflectance standard. The spectra were represented as the Kubelka–Munk function of reflectance, averaging two measurements.

4. Conclusions

In this work a tool, based on QM calculations, was proposed to study the interaction between different organic ligands and the surface metal ions of defective oxides. A thorough computational investigation of the steric and electronic characteristics of TiO_2-based hybrid systems was performed, and a spectroscopic analysis of a set of TiO_2–carboxylate samples assisted the validation of the computational results and the insight into the effect of the molecular structure on the optical absorption and surface redox behaviour of the hybrids. Ti–carboxylate complexes associated with a more favourable interaction energy (namely, citrate, terephthalate and trifluoroacetate) enabled a larger increase of visible light absorption and a more effective surface stabilization of ROS produced by O_2 reduction.

This computational approach allows a rapid screening of large ligand libraries and the prediction of the oxidative activity of the hybrid materials. By optimising the chemical structure of the ligand as well as its interaction with the surface, it is possible to tune the electronic and optical characteristics of the hybrid semiconductor *via* band gap engineering. Indeed, the organic ligand seems to act as a defectivity controller in the sol–gel synthesis of these materials, modifying the surface morphology, promoting the introduction of surface vacancies, and modulating the electronic properties of the product. Therefore, the chemical nature of the ligand is essential to predict these features as well as the resulting photocatalytic efficiency.

We envisage that the proposed approach could be extended to a range of semiconductors and classes of ligands, guiding the design of efficient redox-active materials.

Conflicts of interest

There are no conflicts to declare.

Data availability

All data supporting this study are included in this article and in the ESI.† Any other data, including XYZ structures of QM or PBC calculations, can be obtained from the corresponding author upon reasonable request.

Acknowledgements

G. S., I. R., and L. C. acknowledge the KAUST Supercomputing Laboratory for providing computational resources of the supercomputer Shaheen III, and the Italian MUR for funding through the PRIN2022 project ''MATISSE – A 'Molecular Lift' for the Control of the Metal Protrusion and Coordination Sphere in Single-Atom Catalysts for CO_2 Electroreduction'' (No. 2022K5SX27).

Notes and references

1 B. O'Regan and M. Grätzel, *Nature*, 1991, **353**, 737–740.
2 J. Yu, J. Fan and L. Zhao, *Electrochim. Acta*, 2010, **55**, 597–602.
3 J. Yu, Q. Li and Z. Shu, *Electrochim. Acta*, 2011, **56**, 6293–6298.
4 Y. Bai, I. Mora-Seró, F. De Angelis, J. Bisquert and P. Wang, *Chem. Rev.*, 2014, **114**, 10095–10130.
5 J. Xu, G. Wang, J. Fan, B. Liu, S. Cao and J. Yu, *J. Power Sources*, 2015, **274**, 77–84.
6 Y. Ma, X. Wang, Y. Jia, X. Chen, H. Han and C. Li, *Chem. Rev.*, 2014, **114**, 9987–10043.
7 M. Ismael, *Sol. Energy*, 2020, **211**, 522–546.
8 Y. Shiraishi and T. Hirai, *J. Photochem. Photobiol., C*, 2008, **9**, 157–170.
9 Q.-H. Zhang, W.-D. Han, Y.-J. Hong and J.-G. Yu, *Catal. Today*, 2009, **148**, 335–340.
10 Q. Xu, J. Yu, J. Zhang, J. Zhang and G. Liu, *Chem. Commun.*, 2015, **51**, 7950–7953.
11 J. Bai and B. Zhou, *Chem. Rev.*, 2014, **114**, 10131–10176.
12 P. Amato, M. Fantauzzi, F. Sannino, I. Ritacco, G. Santoriello, M. F. Camellone, C. Imparato, A. Bifulco, G. Vitiello,

L. Caporaso, A. Rossi and A. Aronne, *J. Hazard. Mater.*, 2023, 132907.
13 H. Zhang and J. F. Banfield, *Chem. Rev.*, 2014, **114**, 9613–9644.
14 A. Fujishima and K. Honda, *Nature*, 1972, **238**, 37–38.
15 S. V. Badalov, A. Bocchini, R. Wilhelm, A. L. Kozub, U. Gerstmann and W. G. Schmidt, *Mater. Res. Express*, 2023, **10**, 075501.
16 M. Nunez, B. Forgan and C. Roy, *Int. J. Biometeorol.*, 1994, **38**, 5–17.
17 H. Park, Y. Park, W. Kim and W. Choi, *J. Photochem. Photobiol., C*, 2013, **15**, 1–20.
18 M. Shahrezaei, S. M. H. Hejazi, H. Kmentova, V. Sedajova, R. Zboril, A. Naldoni and S. Kment, *ACS Appl. Mater. Interfaces*, 2023, **15**, 37976–37985.
19 W. Macyk, K. Szaciłowski, G. Stochel, M. Buchalska, J. Kuncewicz and P. Łabuz, *Coord. Chem. Rev.*, 2010, **254**, 2687–2701.
20 C. Gao, J. Wang, H. Xu and Y. Xiong, *Chem. Soc. Rev.*, 2017, **46**, 2799–2823.
21 S. P. Pujari, L. Scheres, A. T. M. Marcelis and H. Zuilhof, *Angew. Chem., Int. Ed.*, 2014, **53**, 6322–6356.
22 T. Tabari, P. Łabuz, A. M. Nowakowska, M. Kobielusz, M. Pacia and W. Macyk, *Dyes Pigm.*, 2023, **213**, 111154.
23 F. Parisi, L. Sciascia, H. Khlifi, L. Elsellami, D. Lenaz, F. Princivalle and F. Parrino, *Ceram. Int.*, 2025, **51**(5), 5494–5504.
24 W. Zhang, W. Huang, J. Jin, Y. Gan and S. Zhang, *Appl. Catal., B*, 2021, **292**, 120197.
25 S. Pang, Y. Lu, L. Cheng, J. Liu, H. Ma, J. Yang and Q. Zhang, *Catal. Sci. Technol.*, 2020, **10**, 3875–3889.
26 J. Park, G. Moon, K.-O. Shin and J. Kim, *Chem. Eng. J.*, 2018, **343**, 689–698.
27 L. A. Almeida, J. Viol, M. Cremona, F. A. F. Menezes, A. O. Guimarães, J. Llorca and B. A. Marinkovic, *J. Photochem. Photobiol., A*, 2024, **452**, 115617.
28 X. Chen, X. Peng, L. Jiang, X. Yuan, J. Zhang and H. Yu, *Colloids Surf., A*, 2020, **603**, 125188.
29 S. Bie, Q. Liu, M. Wen, X. Ye and C. Xiong, *New J. Chem.*, 2021, **45**, 7154–7162.
30 X. Li, H. Xu, J.-L. Shi, H. Hao, H. Yuan and X. Lang, *Appl. Catal., B*, 2019, **244**, 758–766.
31 R. Lakhdar, F. S. Freyria, G. A. Mousdis, B. Bonelli and K. Elghniji, *J. Phys. Chem. C*, 2024, **128**, 13445–13457.
32 I. Ritacco, C. Imparato, L. Falivene, L. Cavallo, A. Magistrato, L. Caporaso, M. Farnesi Camellone and A. Aronne, *Adv. Mater. Interfaces*, 2021, **8**, 2100629.
33 I. Ritacco, G. Gatta, L. Caporaso and M. Farnesi Camellone, *ChemPhysChem*, 2024, **25**(5), DOI: **10.1002/cphc.202300768**.
34 D. Pirozzi, C. Imparato, G. D'Errico, G. Vitiello, A. Aronne and F. Sannino, *J. Hazard. Mater.*, 2020, **387**, 121716.
35 C. Imparato, M. M. Bonifazzi, G. D'Errico, A. Bifulco, O. Tammaro, S. Esposito, A. Aronne and D. Pirozzi, *Colloids Surf., A*, 2024, **684**, 133148.
36 A. Aronne, M. Fantauzzi, C. Imparato, D. Atzei, L. D. Stefano, G. D'Errico, F. Sannino, I. Rea, D. Pirozzi, B. Elsener, P. Pernice and A. Rossi, *RSC Adv.*, 2017, **7**, 2373–2381.
37 L. Rozes, N. Steunou, G. Fornasieri and C. Sanchez, *Monatsh. Chem.*, 2006, **137**, 501–528.
38 V. G. Kessler, G. I. Spijksma, G. A. Seisenbaeva, S. Håkansson, D. H. A. Blank and H. J. M. Bouwmeester, *J. Sol-Gel Sci. Technol.*, 2006, **40**, 163–179.
39 C. Koral, M. Fantauzzi, C. Imparato, G. P. Papari, B. Silvestri, A. Aronne, A. Andreone and A. Rossi, *J. Phys. Chem. C*, 2020, **124**, 23773–23783.
40 E. Carter, A. F. Carley and D. M. Murphy, *J. Phys. Chem. C*, 2007, **111**, 10630–10638.
41 S. Bai, N. Zhang, C. Gao and Y. Xiong, *Nano Energy*, 2018, **53**, 296–336.
42 J. Lim, D. Kwak, F. Sieland, C. Kim, D. W. Bahnemann and W. Choi, *Appl. Catal., B*, 2018, **225**, 406–414.
43 J. Fujisawa, S. Kato and M. Hanaya, *J. Phys. Chem. C*, 2021, **125**, 25075–25086.
44 X. Ma, Y. Shi, Z. Cheng, X. Liu, J. Liu, Z. Guo, X. Cui, X. Sun, J. Zhao, S. Tan and B. Wang, *Nat. Commun.*, 2024, **15**, 2326.
45 J. Fujisawa, S. Kato and M. Hanaya, *Chem. Phys. Lett.*, 2022, **803**, 139833.
46 J. Fujisawa, S. Kato and M. Hanaya, *Chem. Phys. Lett.*, 2023, **827**, 140688.
47 S. V. Badalov, R. Wilhelm and W. G. Schmidt, *J. Comput. Chem.*, 2020, **41**, 1921–1930.
48 M. Setvin, C. Franchini, X. Hao, M. Schmid, A. Janotti, M. Kaltak, C. G. Van de Walle, G. Kresse and U. Diebold, *Phys. Rev. Lett.*, 2014, **113**, 086402.
49 J.-L. Shi, H. Hao, X. Li and X. Lang, *Catal. Sci. Technol.*, 2018, **8**, 3910–3917.
50 C. Imparato, G. D'Errico, W. Macyk, M. Kobielusz, G. Vitiello and A. Aronne, *Langmuir*, 2022, **38**, 1821–1832.
51 U. Schubert, *J. Mater. Chem.*, 2005, **15**, 3701–3715.
52 S. Barboux-Doeuff and C. Sanchez, *Mater. Res. Bull.*, 1994, **29**, 1–13.
53 D. P. Birnie III and N. J. Bendzko, *Mater. Chem. Phys.*, 1999, **59**, 26–35.
54 B. S. Buyuktas and O. Aktas, *Transition Met. Chem.*, 2006, **31**, 56–61.
55 I. D. Varma and R. C. Mehrotra, *J. Prakt. Chem.*, 1959, **8**, 235–240.
56 F. Babonneau, S. Doeuff, A. Leaustic, C. Sanchez, C. Cartier and M. Verdaguer, *Inorg. Chem.*, 1988, **27**, 3166–3172.
57 R. Parra, M. S. Góes, M. S. Castro, E. Longo, P. R. Bueno and J. A. Varela, *Chem. Mater.*, 2008, **20**, 143–150.
58 I. Mijatovic, G. Kickelbick, M. Puchberger and U. Schubert, *New J. Chem.*, 2003, **27**, 3–5.
59 A. Leaustic, F. Babonneau and J. Livage, *Chem. Mater.*, 1989, **1**, 240–247.
60 R. J. Errington, J. Ridland, W. Clegg, R. A. Coxall and J. M. Sherwood, *Polyhedron*, 1998, **17**, 659–674.
61 L.-F. Liao, C.-F. Lien and J.-L. Lin, *Phys. Chem. Chem. Phys.*, 2001, **3**, 3831–3837.
62 S. Doeuff, M. Henry, C. Sanchez and J. Livage, *J. Non-Cryst. Solids*, 1987, **89**, 206–216.

63 F. X. Perrin, V. Nguyen and J. L. Vernet, *J. Sol-Gel Sci. Technol.*, 2003, **28**, 205–215.
64 S. Sun, P. Song, J. Cui and S. Liang, *Catal. Sci. Technol.*, 2019, **9**, 4198–4215.
65 N. Tiwale, A. Subramanian, Z. Dai, S. Sikder, J. T. Sadowski and C.-Y. Nam, *Commun. Mater.*, 2020, **1**, 94.
66 T. Berger, M. Sterrer, O. Diwald, E. Knözinger, D. Panayotov, T. L. Thompson and J. T. Yates, *J. Phys. Chem. B*, 2005, **109**, 6061–6068.
67 P. Amato, M. Fantauzzi, F. Sannino, I. Ritacco, G. Santoriello, M. Farnesi Camellone, C. Imparato, A. Bifulco, G. Vitiello, L. Caporaso, A. Rossi and A. Aronne, *J. Hazard. Mater.*, 2024, **463**, 132907.
68 D. G. Calatayud, T. Jardiel, M. Peiteado, C. Fernández Rodríguez, M. R. E. Estévez, J. M. D. Rodríguez, F. J. Palomares, F. Rubio, D. Fernández-Hevia and A. C. Caballero, *J. Mater. Chem. A*, 2013, **1**, 14358–14367.
69 I. A. Mudunkotuwa and V. H. Grassian, *J. Am. Chem. Soc.*, 2010, **132**, 14986–14994.
70 Z. Guo, C. Li, S. Lu, Y. Pan and H. Gu, *RSC Adv.*, 2015, **5**, 74230–74237.
71 M. Chiesa, E. Giamello and M. Che, *Chem. Rev.*, 2010, **110**, 1320–1347.
72 E. Carter, A. F. Carley and D. M. Murphy, *J. Phys. Chem. C*, 2007, **111**, 10630–10638.
73 M. L. Addonizio, A. Aronne and C. Imparato, *Appl. Surf. Sci.*, 2020, **502**, 144095.
74 K. Qi, F. Zasada, W. Piskorz, P. Indyka, J. Gryboś, M. Trochowski, M. Buchalska, M. Kobielusz, W. Macyk and Z. Sojka, *J. Phys. Chem. C*, 2016, **120**, 5442–5456.
75 J. Fujisawa, S. Kato and M. Hanaya, *J. Phys. Chem. C*, 2024, **128**, 11247–11254.
76 C. Zhang, Y. Li, M. Li, D. Shuai, X. Zhou, X. Xiong, C. Wang and Q. Hu, *J. Hazard. Mater.*, 2021, **420**, 126607.
77 M. J. Frisch, G. W. Trucks, H. B. Schlegel, G. E. Scuseria, M. A. Robb, J. R. Cheeseman, G. Scalmani, V. Barone, G. A. Petersson, H. Nakatsuji, X. Li, M. Caricato, A. V. Marenich, J. Bloino, B. G. Janesko, R. Gomperts, B. Mennucci, H. P. Hratchian, J. V. Ortiz, A. F. Izmaylov, J. L. Sonnenberg, D. Williams-Young, F. Ding, F. Lipparini, F. Egidi, J. Goings, B. Peng, A. Petrone, T. Henderson, D. Ranasinghe, V. G. Zakrzewski, J. Gao, N. Rega, G. Zheng, W. Liang, M. Hada, M. Ehara, K. Toyota, R. Fukuda, J. Hasegawa, M. Ishida, T. Nakajima, Y. Honda, O. Kitao, H. Nakai, T. Vreven, K. Throssell, J. A. Montgomery, Jr., J. E. Peralta, F. Ogliaro, M. J. Bearpark, J. J. Heyd, E. N. Brothers, K. N. Kudin, V. N. Staroverov, T. A. Keith, R. Kobayashi, J. Normand, K. Raghavachari, A. P. Rendell, J. C. Burant, S. S. Iyengar, J. Tomasi, M. Cossi, J. M. Millam, M. Klene, C. Adamo, R. Cammi, J. W. Ochterski, R. L. Martin, K. Morokuma, O. Farkas, J. B. Foresman and D. J. Fox, *Gaussian 16, Revision C.01*, Gaussian, Inc., Wallingford CT, 2016.
78 A. D. Becke, *J. Chem. Phys.*, 1993, **98**, 5648–5652.
79 R. Ditchfield, W. J. Hehre and J. A. Pople, *J. Chem. Phys.*, 1971, **54**, 724–728.
80 V. Barone and M. Cossi, *J. Phys. Chem. A*, 1998, **102**, 1995–2001.
81 Y. Zhao and D. G. Truhlar, *Theor. Chem. Acc.*, 2008, **120**, 215–241.
82 F. Weigend and R. Ahlrichs, *Phys. Chem. Chem. Phys.*, 2005, **7**, 3297–3305.
83 S. W. Benson, *The Foundations of Chemical Kinetics*, R. E. Krieger, Malabar FL, 1982.
84 D. Ardura, R. López and T. L. Sordo, *J. Phys. Chem. B*, 2005, **109**, 23618–23623.
85 P. Giannozzi, S. Baroni, N. Bonini, M. Calandra, R. Car, C. Cavazzoni, D. Ceresoli, G. L. Chiarotti, M. Cococcioni, I. Dabo, A. D. Corso, S. de Gironcoli, S. Fabris, G. Fratesi, R. Gebauer, U. Gerstmann, C. Gougoussis, A. Kokalj, M. Lazzeri, L. Martin-Samos, N. Marzari, F. Mauri, R. Mazzarello, S. Paolini, A. Pasquarello, L. Paulatto, C. Sbraccia, S. Scandolo, G. Sclauzero, A. P. Seitsonen, A. Smogunov, P. Umari and R. M. Wentzcovitch, *J. Phys.: Condens. Matter*, 2009, **21**, 395502.
86 J. P. Perdew, K. Burke and M. Ernzerhof, *Phys. Rev. Lett.*, 1996, **77**, 3865–3868.
87 D. Vanderbilt, *Phys. Rev. B: Condens. Matter Mater. Phys.*, 1990, **41**, 7892–7895.
88 P. M. Kowalski, M. F. Camellone, N. N. Nair, B. Meyer and D. Marx, *Phys. Rev. Lett.*, 2010, **105**, 146405.